Published in final edited form as:
Biol Psychiatry. 2014 September 1; 76(5): 387–396. doi:10.1016/j.biopsych.2013.08.018.

The dyslexia-associated gene Dcdc2 is required for spike-timing precision in mouse neocortex

Alicia Che, **Matthew J. Girgenti**, and **Joseph LoTurco**
Department of Physiology and Neurobiology, University of Connecticut, Storrs, CT 06269

Abstract

Background—Variants in dyslexia-associated genes, including DCDC2, have been linked to altered neocortical activation, suggesting that dyslexia associated genes may play as of yet unspecified roles in neuronal physiology.

Methods—Whole-cell patch clamp recordings were used to compare the electrophysiological properties of regular spiking (RS) pyramidal neurons of neocortex in Dcdc2 knock out (KO) and wild-type (WT) mice. RNA-seq and RT-PCR were performed to identify and characterize changes in gene expression in Dcdc2 KOs.

Results—Neurons in KOs showed increased excitability and decreased temporal precision in action potential (AP) firing. The RNA-seq screen revealed that the N-methyl-D-aspartate receptor (NMDAR) subunit Grin2B was elevated in Dcdc2 KOs, and an electrophysiological assessment confirmed a functional increase in spontaneous NMDAR-mediated activity. Remarkably, the decreased AP temporal precision could be restored in mutants by treatment with either the NMDAR antagonist APV or the NMDAR 2B subunit (NR2B)-specific antagonist Ro 25-6981.

Conclusions—These results link the function of the dyslexia-associated gene Dcdc2 to spike timing through activity of NMDAR.

Keywords

dyslexia; Dcdc2; Grin2B; spike-time precision; excitability; neocortex

Introduction

Developmental dyslexia is caused by a still poorly understood interaction between genetic and environmental factors (1–2). Single gene association studies and subsequent meta-analyses provide relatively strong evidence for association between variants of genes on

Corresponding Author: Joe LoTurco, Department of Physiology and Neurobiology, University of Connecticut, Storrs, CT 06269-3156, Phone: 860-486-3271, Joseph.LoTurco@uconn.edu.

Financial Disclosures
The authors report no biomedical financial interests or conflicts of interest.

chromosome 6p21.3, including DCDC2 and KIAA0319, and risk for developmental dyslexia (3–6). In addition, recent neuroimaging experiments demonstrate that variants of both DCDC2 and KIAA0319 also associate with alterations in neocortical activation during reading related tasks (7–10). One hypothesis emerging from these findings is that dyslexia associated genes may function in the neurophysiology of neocortical circuits.

Results of previous *in utero* RNAi experiments show that targeting expression of either Kiaa0319 or Dcdc2 in fetal rat somatosensory neocortex causes a displacement of neocortical pyramidal neurons in neocortical circuits by disrupting neuronal migration (3,11). Recent studies now show that neuronal migration is neither an essential nor the sole function of Kiaa0319 or Dcdc2 in the cortex. For example, in Dcdc2 KO mice there are no apparent disruptions in neuronal migration or displacement of neurons in neocortical circuits (12–13). In spite of normal neocortical patterning, Dcdc2 KOs display behavioral deficits in performing novel object recognition tasks, and in learning difficult versions of the Hebb-Williams maze (13). In addition, RNAi targeting Kiaa0319 in developing auditory neocortex does not result in significant displacement of neurons, but nevertheless results in alterations in neurophysiological responses to speech stimuli, and in elevated excitability of neocortical pyramidal neurons (14). Together, these results suggest effects of dyslexia-associated genes that go beyond disruption in neuronal migration and may connect their function to cellular neurophysiology.

In this study we sought to determine whether the genetic loss of Dcdc2 is associated with measureable cellular neurophysiological changes in pyramidal neurons of mouse neocortex. In the initial characterization we focused on properties of AP rate and AP timing, and found consistently heightened excitability and altered spike-time precision in pyramidal neurons in KOs. High throughput RNA-sequencing of the WT and KOs revealed up-regulation of the 2B subunit of NMDAR, Grin2B, and blocking NMDARs restored measures of temporal precision in KO neurons to WT levels. Our results indicate that Dcdc2 functions in maintaining temporal coding in neocortical neurons by regulating the expression and function of NMDARs in neocortical pyramidal neurons.

Materials and Methods

Slice Preparation

P18–P28 WT and Dcdc2 KO mice were deeply anesthetized with isoflurane and then decapitated. All experiments were performed under the approval of the University of Connecticut Animal Care and Use Committee. Brains were rapidly removed and immersed in ice-cold oxygenated (95% O_2 and 5% CO_2) dissection buffer containing (in mM): 83 NaCl, 2.5 KCl, 1 NaH_2PO_4, 26.2 $NaHCO_3$, 22 glucose, 72 sucrose, 0.5 $CaCl_2$, and 3.3 $MgCl_2$. Coronal slices (400 μm) were cut using a vibratome (VT1200S, Leica), incubated in dissection buffer for 40 min at 34°C, and then stored at room temperature for reminder of the recording day. All slice recordings were performed at 34°C. Slices were visualized using IR differential interference microscopy (DIC) (E600FN, Nikon) and a CCD camera (QICAM, QImaging). Individual neurons were visualized with a 40x Nikon Fluor water immersion (0.8 NA) objective.

Electrophysiology

For all experiments, extracellular recording buffer was oxygenated (95% O_2 and 5% CO_2) and contained (in mM): 125 NaCl, 25 $NaHCO_3$, 1.25 NaH_2PO_4, 3 KCl, 25 dextrose, 1 $MgCl_2$, and 2 $CaCl_2$. Patch pipettes were fabricated from borosilicate glass (N51A, King Precision Glass, Inc.) to a resistance of 2–5 MΩ. The resultant errors were minimized with bridge balance and capacitance compensation. For current-clamp experiments and slope current measurement, pipettes were filled with an internal solution containing (in mM): 125 potassium gluconate, 10 HEPES, 4 Mg-ATP, 0.3 Na-GTP, 0.1 EGTA, 10 2-Tris-phosphocreatine, 0.05% biocytin, adjusted to pH 7.3 with KOH and to 278 mOsm with double-distilled H_2O. Signals were amplified with a Multiclamp 700A amplifier (Molecular Devices), digitized (ITC-18, HEKA Instruments Inc.) and filtered at 2 kHz. Data were monitored, acquired and in some cases analyzed using Axograph X software. Series resistance was monitored throughout the experiments by applying a small test voltage step and measuring the capacitive current. Series resistance was 5~25 MΩ and only cells with <20% change in series resistance and holding current were included in the analysis. Reported membrane potentials and holding potentials were not corrected for liquid junction potential unless otherwise specified.

For excitability measurements, 500 ms current steps were applied at 50 pA increments from −300 pA to 500 pA. Numbers of APs per 500 ms were only quantified for steps 250 pA and above to ensure all WT and KO cells were above firing threshold. For all spike-timing experiments, GABAa receptors were blocked with SR-95531 (Gabazine, 5μM, Ascent Scientific), and RMP was adjusted to −75 mV for all cells by injecting a small current. Amplitudes of dc current steps were adjusted for individual cells to obtain 12 spikes in 500 ms. This firing rate was chosen based on input-output relations observed for cells recorded – 12 APs could be reliably achieved in all WT and KO neurons by applying 200 – 450 pA current. spike trains were repeatedly generated for 10 to 20 times with 14.5 s between trials for each cell. Noise stimuli were generated in Matlab (Mathworks) according to methods used by Mainen et al., which consisted of a Gaussian white noise with mean (μ_s) = 200 pA and SD (σ_s) = 100 pA, convolved with the function $f(t) = t \exp(-t/\tau_s)$ with time constant τ_s = 3 ms to simulate synaptic integration (15). The step duration in these experiments was 1 s. In specified experiments, DL-2-amino-5-phosphopentanoic acid (DL-AP5, 100 μM, Ascent Scientific) was used to block NMDARs, Ro25-6981 (0.5 μM, Ascent Scientific) to block specifically NMDAR 2B subunits (NR2Bs), and 2,3,dioxo-6-nitro-1,2,3,4,tetrahydrobenzo-quinoxaline-7-sulfonamide (NBQX, 10 μM, Ascent Scientific) to block AMPARs.

For spontaneous NMDA activity measurements, internal solution used contained (in mM): 110 $CsMeSO_4$, 10 CsCl, 10 HEPES, 10 Cs_4-BAPTA, 5 QX-314•Br, 0.1 spermine, 4 Mg-ATP, 0.4 Na-ATP, 10 2-Tris-phosphocreatine, 0.05% biocytin, adjusted to pH 7.3 with KOH to 278 mOsm with double-distilled H_2O. Recordings began at least 10 min after initial whole cell recording to allow dialysis of Cs^+ internal solution. Cells were voltage-clamped at +40 mV in the presence of NBQX (10 μM) and tetrodotoxin (TTX, 1 μM, Ascent Scientific). GABAa receptors were blocked with SR-95531 (Gabazine, 5μM, Ascent Scientific). DL-APV (100 μM) washes were 8 – 10 minutes in duration, and 180 s

recordings before and after (while DL-APV application continued) were used for spontaneous phasic event analysis.

Data Analysis and Statistics

APs were detected using either Axograph X built-in data analysis package or IGOR Pro software (Wavemetrics) on a Macintosh computer. AP shape analyses were performed according to previously established criteria (16). Detailed methods on AP shape, membrane properties and conductance measurements are included in Supplement 1.

In spike-timing experiments, rastergrams were generated using Igor Pro software. Inter-spike interval (ISI) was calculated by subtracting the time when the AP peak occurs by that of the previous AP for each spike train. Instantaneous firing rate was calculated as the inverse of ISI and plotted against the peak time of the first spike in the pair. ISI histogram was generated by sorting peak time of spikes from all spike trains, and plotting ISI between two subsequent spikes. Each spike in a train, or spike alignment across all trials, was classified as an event. Jitter of an event was quantified as the standard deviation (SD) of times at which AP peaks occur from all trials at that particular event. Temporal jitter and jitter histograms represented the average jitter of all cells at the n^{th} event:

$$\mathrm{Jitter}_{\mathrm{nth}}=\frac{\mathrm{Cell\,1\,jitter}_{\mathrm{nth}}+\mathrm{Cell\,2\,jitter}_{\mathrm{nth}}+\ldots+\mathrm{Cell\,N\,jitter}_{\mathrm{nth}}}{\mathrm{N}}$$

where N is the number of cells recorded.

Coefficient of variance (CV) of the n_{th} inter-stimulus-interval (ISI) was quantified by dividing the standard deviation (SD) of ISIs between two events by their mean across all trials. Similar methods histograms as described for jitter quantification were used to construct CV.

To detect phasic spontaneous NMDAR-mediated events, a variable amplitude template was slid through 180 s chart recordings (17). The parameters of the template, including amplitude, 10–90% rise time, and decay time, were determined based on an average of real events as well as previously reported values. The detection threshold is 4 to 9 times of the noise standard deviation. Events detected were in some cases verified manually. Tonic current is measured by subtracting the mean current response recorded before and after the application of DL-APV. Statistics were performed using Excel (Microsoft) and Prism 6 software (Graphpad), and graphs were generated in IGOR Pro software (Wavemetrics). Statistical significance was determined using either two-tailed Student's t-Test (indicated on figures with asterisks) or repeated measures ANOVA. Significance was based on *P* values < 0.05. Means and standard errors were reported for all results unless otherwise specified.

RNA-seq Analysis

Methods are included in Supplement 1.

Results

Increased spike rate and decreased spike timing precision in Dcdc2 KOs

Neuronal spike rates and temporal patterns together encode stimulus features and stimulus change (18–21). We therefore assessed both spike rate and spike time precision in neocortical pyramidal neurons in WT and Dcdc2 KOs. The rates of APs generated by a range of supra-threshold current steps were significantly increased in KO neurons compared to WT neurons [repeated measures ANOVA (between variables: genotype; within variables: current step), main effect of genotype: $F(1, 36) = 9.34$, $P < 0.005$; WT, n = 16; KO, n = 22] (Figure 1A and B). In addition, KO neurons had more depolarized RMPs [$t(44) = 3.61$, $p < 0.001$], and elevated input resistances relative to WT [$t(44) = 2.34$, $P < 0.05$], but were not significantly different from WT in AP voltage threshold [$t(20) = 0.87$, NS], amplitude [$t(20) = 0.16$, NS] or width [$t(20) = 1.08$, NS] (Table 1).

In order to assess whether spike temporal precision was altered in Dcdc2 KO neurons, we repeatedly presented supra-threshold depolarizing current steps to neurons with pre-stimulus RMPs adjusted to −75 mV. Spike rastergrams from 10 to 20 repeated stimulus trials were then used to calculate the temporal jitter in the timing of each AP. As an additional related measure of temporal precision, CV for each ISI was also calculated (19). Dcdc2 KOs (n=10) showed far less AP temporal precision than WT (n = 10) neurons (Figure 1C–F, right). Temporal jitter was significantly elevated in KOs [repeated measures ANOVA (between variables: genotype; within variables: event), genotype x event interaction: $F(11, 198) = 8.38$, $p < 0.0001$, Figure 1G; main effect of genotype: $F(1,18) = 12.14$, $P < 0.005$, Figure 1H]. Similarly, CVs of ISIs were significantly elevated in KO relative to WT throughout the duration of stimulation [repeated measures ANOVA (between variables: genotype; within variables: event) followed by Holm-Sidak's test, difference significant between genotypes for each of the 11 ISI events, Figure 1I; main effects of genotype: $F(1,18) = 22.76$, $P < 0.001$, Figure 1J]. The results indicate that KO neurons exhibit increased spike rates and decreased spike-time temporal precision.

Increased spike rate is due to elevated RMP while decreased temporal precision is not

Our comparison identified three changes in electrophysiological parameters in KO relative to WT neurons: elevated membrane potential, increased spike rate, and decreased temporal precision. In order to determine whether the elevation in RMP was responsible for elevated spike rate, we performed an additional set of current clamp recordings in KO neurons (n=14) in which the membrane potential of each KO neuron was set to the average RMP of WT neurons, −75 mV, by injection of a hyperpolarizing rheobase. When repolarized to −75 mV, the firing rates of KO neurons were no longer significantly different from WT neurons [repeated measures ANOVA (between variables: genotype; within variables: current step), main effect of genotype: $F(1,28) = 0.029$, NS] (Figure 1B). In contrast to the effect on spike rate, adjustment of RMPs in KO neurons to WT levels did not reduce the average CV of spike timing nor did it reduce temporal jitter in KOs to WT levels (Figure 2). Consistent with this dissociation, the average temporal jitter [repeated measures ANOVA (between variables: genotype; within variables: current step), main effect of genotype: $F(1,16) = 16.14$, $P < 0.001$; followed by Holm-Sidak's test, difference significant between genotypes

for every current step] and CV collapsed from all ISIs in KOs were consistently higher relative to WT at every spike rate tested [repeated measures ANOVA (between variables: genotype; within variables: current step), main effect of genotype: $F(1,16) = 9.62$, $P < 0.01$; followed by Holm-Sidak's test, difference significant between genotypes for every current step] (WT, n = 9; KO, n = 9, Figure 2A,B). Furthermore, RMP did not significantly correlate with average temporal jitter in either WT or KO neurons [linear regression of WT at 300 pA: $R^2 = 0.00085$; WT at 500 pA: $R^2 = 0.015$; KO at 300 pA: $R^2 = 0.29$; KO at 500 pA: $R^2 = 0.014$] (WT, n = 9; KO, n = 9; Figure 2C,D). These results together indicate that changes in spike rate and membrane depolarization observed in the KO were not responsible for changes in AP temporal precision in KO neurons.

Grin2B expression is elevated in Dcdc2 KOs and blocking Grin2B receptors restores spike time precision

In an effort to identify changes in ion channels or receptors that may be responsible for the underlying electrophysiological changes that could degrade spike-time precision in Dcdc2 KOs, we performed a whole-transcriptome RNA-seq comparison of WT and KO neocortex at P21 (Figure 3A). A total of 155 transcripts were found to be up-regulated by 2-fold or more (Supplement: Table S2), and 113 transcripts were found to be down-regulated by 2-fold or more in KO relative to WT neocortex (Supplement: Table S3). We searched the lists for ion channels that could be implicated in spike-time precision (i.e. voltage gated potassium channels or neurotransmitter receptors) and found that the most up-regulated transcript that encoded an ion channel or receptor was Grin2B, the 2B subunit of NMDAR (Figure 3A; Supplement: Table S2). We confirmed that Grin2B was up-regulated in a follow-up qRT-PCR experiment (n=6, Figure 3B). The possibility that elevated NMDAR-mediated currents could be involved in degrading temporal precision was shown previously in dynamic clamp experiments in which injected NMDAR-like conductances decreased temporal precision in neocortical pyramidal neurons (22). To test whether elevated Grin2B contributed to spike timing changes, we examined the effect of bath applying the NR2B-specific blocker Ro 25-6981 (0.5 μM) to KO neurons (n = 7). We found that Ro 25-6981, similar to the pan NMDAR blocker DL-APV (see below), significantly increased measures of temporal precision in KO neurons [repeated measures ANOVA (matching: event and treatment), main effect of treatment: $F(1,6) = 9.40$, $P < 0.01$], and resulted in CVs of ISIs in KO neurons that did not significantly differ from WT neurons [repeated measures ANOVA (between variables: genotype; within variables: event), main effect of genotype: $F(1,15) = 4.06$, NS] (Figure 3C,D).

Tonic and phasic NMDAR activity is elevated in Dcdc2 KOs

We next tested for increases in NMDAR activity by directly measuring spontaneous NMDAR activity in voltage clamp. There are two types of spontaneous NMDAR currents in cortical neurons, a phasic current that reflects the discrete synaptic release of glutamate, and a tonic current that reflects activation of NMDARs by ambient glutamate (23–24). To determine whether these spontaneous NMDAR conductances were elevated in Dcdc2 KO neurons, we isolated spontaneous NMDAR-mediated currents pharmacologically (SR-95531 and NBQX) and relieved voltage-dependent magnesium block by holding the membrane potential at +40 mV in physiological extracellular magnesium concentrations. We found a

significant increase in the frequency [1.46 ± 0.24 Hz in KO vs. 0.65 ± 0.12 in WT; t (22) = 2.46, $P < 0.05$] (Figure 4A–C), but not amplitude [10.69 ± 0.86 pA in KO vs. 8.76 ± 0.75 pA in WT; t (22) = 1.54, NS, Figure 4D], rise time [4.19 ± 0.15 ms in KO vs. 4.16 ± 0.29 in WT; t (22) = 0.13, NS, Figure 4E] or decay time [38.79 ± 1.18 ms in KO vs. 39.45 ± 1.09 in WT; t (22) = 0.38, NS, Figure 4F] of phasic NMDAR-mediated currents in KOs relative to WT (WT, n = 9; KO, n = 15). The tonic NMDAR current, measured by the change in steady-state current amplitude after APV application, was also increased in KOs relative to WT neurons (47.2 ± 6.2 pA in KO, n =8; 23.3 ± 4.1 in WT, n = 8; t (14) = 3.23, $P < 0.01$. Figure 4G,H).

Blockade of NMDARs but not AMPARs Restores Spike-time Precision

We next tested whether the effect on AP temporal precision in KOs was specific to blockade of the NMDA class of glutamate receptors. We compared the effects of the pan-NMDAR antagonist APV with effects of the non-NMDA glutamate receptor antagonist NBQX in both KO and WT neurons. In Dcdc2 KO neurons blocking NMDARs with DL-APV (100 μM) was, similar to the effects of the NR2B specific antagonist, effective at reducing CVs [repeated measures ANOVA (matching: event and treatment), main effect of treatment: F (1,9) = 40.26, $P < 0.005$] and returning AP timing precision to WT levels [repeated measures ANOVA (between variables: genotype; within variables: event), main effect of genotype: F (1,18) = 0.67, NS] (n = 10, Figure 5A,H,C). In contrast, blockade of the non-NMDA glutamate receptors (AMPARs) by NBQX (10 μM) had no significant effect on the temporal precision of AP timing in Dcdc2 KOs [repeated measures ANOVA (matching: event and treatment), main effects of treatment: F (1,9) = 0.16, NS] (n = 10, Figure 5B,D). Thus, the rescue of AP temporal precision in KOs is specific to the NMDA class of glutamate receptors.

Blockade of NMDARs restores spike-time precision in response to stationary noise

Neurons *in vivo* typically receive stimulation from relatively noisy barrages of synaptic currents. We therefore assessed whether the temporal precision changes in KO were apparent to noisy stimuli typical of *in vivo* synaptic inputs. The stimulus applied was a filtered Gaussian distribution designed previously to approximate the rapid fluctuation of membrane potentials resulting from the integration of many synaptic events (15; 25). Similar to previous reports, fluctuating noise stimuli elicited spike timing with higher temporal precision than did square wave current stimulation (Figure 6A). Even with these noisy stimuli that produce more temporally precise patterns of APs, KO neurons showed significantly less precise spike timing than WT neurons (Figure 6B). Moreover, similar to the changed response to square wave stimuli, APV significantly reduced both measures of temporal precision, jitter [repeated measures ANOVA (between variables: genotype; within variables: treatment), genotype x treatment interaction: F (1,14) = 9.40, $P < 0.01$; followed by Sidak's test, difference significant between genotypes pre APV, no significance in APV] and CV [repeated measures ANOVA (between variables: genotype; within variables: treatment), genotype x treatment interaction: F (1,14) = 13.34, $P < 0.005$; followed by Sidak's test, difference significant between genotypes pre APV, no significance in APV] in KO neurons to WT levels (Figure 6C–F).

Discussion

Several electrophysiological properties influence the temporal precision of APs in central neurons, including nonlinearity of membrane conductances at threshold (26–28) and synaptic noise (29–30). Spontaneous synaptic noise can either enhance or reduce the temporal precision of spike trains depending on their features [review see (31)]. In cortical RS neurons specifically, the type of background synaptic conductance added can affect the gain and variability in the timing of APs elicited by depolarizing inputs (22,30,32–33). We show that in Dcdc2 KO mice, cortical RS neurons have higher trial-to-trial spike-time variability, elevated NMDA conductances and spike timing can be returned to WT levels by blocking NMDARs. Our results show that change in endogenous NMDAR activity, which can occur in many physiological (34–36) and pathological states (37–38), can result in altered spike-time temporal precision.

In addition to impaired spike-time precision, our findings show that deletion of Dcdc2 results in heightened excitability associated with depolarized RMP. In recent years, changes in intrinsic excitability of neurons as a type of non-synaptic plasticity have been shown to link to learning, and can be both synaptically driven or independent of synaptic stimulation [review see (39)]. Heightened cell excitability is often associated with more extreme pathology (39–41), but smaller changes in excitability could be related to degradation in sensory processing. For example, *In utero* RNAi of Kiaa0319 in rat neocortex has been recently shown to cause elevated excitability of neocortical pyramidal neurons (14). This elevation in excitability caused by Kiaa0319 RNAi is also associated with less precise neural encoding of auditory stimuli (14). Regulation of neuronal excitability may be a common function of Dcdc2 and Kiaa0319.

Although dyslexia is primarily a language-specific learning disorder, there is evidence that the underlying neurological changes may be dissociable from language, and associated with more generalized changes in temporal and high-level sensory processing (42–44). Several cognitive changes that do not directly involve reading have been linked to dyslexia, including changes in event-related potentials (45) and fMRI responses to non-word stimuli (46), as well as alterations in general sensory stimulus sampling (42, 47–48). It has been theorized that the general temporal processing deficits are associated with abnormal cortical firing (49–50), and precise spike timing may contribute to high speed population coding and synchronization (51) as well as enhance discrimination of stimuli (52). Our study indicates the possible link between a dyslexia-associated gene, Dcdc2, and a cellular physiological dysfunction in spike-time precision that could be the basis for changes in temporal processing on a system level.

Dcdc2 is one of the 11-member doublecortin (DCX) gene family, whose molecular functions are mostly inferred from the DCX domain and its ability to bind microtubules (53). Although Dcdc2 biochemically interacts with tubulin and JIP 1/2 (54), its molecular role remains elusive. Members of DCX families have been shown to be involved in neuronal migration, intracellular transport, and cell signaling through protein-protein interaction (55). Given the specific increase in NMDAR-mediated activity and Grin2B expression in Dcdc2 KO mice, it is possible that Dcdc2 is involved in homeostatic Grin2B transcript up-

regulation. The mRNA up-regulation of Grin2B in KOs also suggests the possibility that Dcdc2 acts as a co-repressor or RNA binding protein that destabilizes Grin2B, regulating Grin2B transcript levels directly. In fact, some members of the DCX-family can localize to the nucleus and Dcdc2 itself has a domain consistent with possible nuclear localization. Future studies will test these hypotheses by investigating interactions between Dcdc2 and known proteins involved in the transport of NR2B protein or Grin2B transcript, cellular localization of Dcdc2, and potential link between Dcdc2 and regulatory regions on Grin2B.

Our study demonstrates that a genetic manipulation of a dyslexia-associated gene leads to increases in NMDAR activity. Several possibilities may account for this elevated activity: 1) an increased number of postsynaptic NMDARs; 2) an increased number of synapses; 3) increased ambient glutamate concentration; 4) an increased number of presynaptic NMDARs [comprised of mostly NR1/NR2B in the cortex after early postnatal stages (56–58)], which leads to higher transmitter release probability from the presynaptic terminals. Elevated Grin2B mRNA expression level and potential functional changes associated with this increase (such as altered NMDAR subunit composition, change in receptor distribution, or change in developmental switch) does not directly provide evidence for favoring one of the above listed possibilities. Therefore, considering the dynamic regulation of NMDARs and its subunits, further work needs to be done to identify the specific cause of increased NMDAR activity, particularly in relation to elevated Grin2B expression level.

It is interesting to note that short-term memory for words in individuals with RD has been found to link to variants in GRIN2B (59). NMDAR activation is well known for its positive role in synaptic plasticity and learning. Intriguingly, increased NMDAR activity would be predicted to enhance plasticity at synapses by Hebbian mechanisms, but at the same time decreased spike-timing precision would tend to decrease Hebbian plasticity in a network. This balance may be a homeostatic change to counter spurious spike-timing dependent plasticity in networks that could result from elevated NMDAR activity. Alternatively, a network with greater synaptic plasticity but with increased spike-time variability may be more dynamic in terms of new patterns that can be stored.

Supplementary Material

Refer to Web version on PubMed Central for supplementary material.

Acknowledgments

We thank Dr. Anastasios Tzingounis for helpful discussions and for comments on the manuscript. We thank Dr. Xinnian Chen and Mr. Takumi Otsuka for assistance with Matlab simulation, and Ms. Dongnhu Truong for help with statistical analyses. This research is supported by NIH grants R01HD055655, R01MH056524, and P01HD057853.

References

1. Rosenberg J, Pennington BF, Willcutt EG, Olson RK. Gene by environment interactions influencing reading disability and the inattentive symptom dimension of attention deficit/hyperactivity disorder. Journal of child psychology and psychiatry, and allied disciplines. 2012; 53:243–251.
2. Peterson RL, Pennington BF. Developmental dyslexia. The Lancet. 2012

3. Meng H, Smith SD, Hager K, Held M, Liu J, Olson RK, et al. DCDC2 is associated with reading disability and modulates neuronal development in the brain. Proc Natl Acad Sci USA. 2005; 102:17053–17058. [PubMed: 16278297]
4. Schumacher J, Anthoni H, Dahdouh F, König IR, Hillmer AM, Kluck N, et al. Strong Genetic Evidence of DCDC2 as a Susceptibility Gene for Dyslexia. The American Journal of Human Genetics. 2006; 78:52–62.
5. Zou L, Chen W, Shao S, Sun Z, Zhong R. Genetic variant in KIAA0319, but not in DYX1C1, is associated with risk of dyslexia: An integrated meta analysis. Am J Med Genet. 2012; 159B:970–976. [PubMed: 23065966]
6. Zhong R, Yang B, Tang H, Zou L, Song R, Zhu LQ. Meta-analysis of the Association Between DCDC2 Polymorphisms and Risk of Dyslexia. Molecular Neurobiology. 2013; 47:435–442. [PubMed: 23229871]
7. Cope N, Eicher JD, Meng H, Gibson CJ, Hager K. Variants in the DYX2 locus are associated with altered brain activation in reading-related brain regions in subjects with reading disability. Neuroimage. 2012; 63:148–156. [PubMed: 22750057]
8. Darki F, Peyrard-Janvid M, Matsson H, Kere J, Klingberg T. Three dyslexia susceptibility genes, DYX1C1, DCDC2, and KIAA0319, affect temporo-parietal white matter structure. Biological Psychiatry. 2012; 72:671–676. [PubMed: 22683091]
9. Meda SA, Gelernter J, Gruen JR, Calhoun VD, Meng H, Cope NA, Pearlson GD. Polymorphism of DCDC2 Reveals Differences in Cortical Morphology of Healthy Individuals—A Preliminary Voxel Based Morphometry Study. Brain Imaging and Behavior. 2007; 2:21–26. [PubMed: 19096528]
10. Pinel P, Fauchereau F, Moreno A, Barbot A, Lathrop M, Zelenika D, et al. Genetic Variants of FOXP2 and KIAA0319/TTRAP/THEM2 Locus Are Associated with Altered Brain Activation in Distinct Language-Related Regions. J Neurosci. 2012; 32:817–825. [PubMed: 22262880]
11. Paracchini S, Thomas A, Castro S, Lai C. The chromosome 6p22 haplotype associated with dyslexia reduces the expression of KIAA0319, a novel gene involved in neuronal migration. Human Molecular Genetics. 2006; 15:1659–1666. [PubMed: 16600991]
12. Wang Y, Yin X, Rosen G, Gabel L, Guadiana SM, Sarkisian MR, et al. Dcdc2 knockout mice display exacerbated developmental disruptions following knockdown of doublecortin. Neuroscience. 2011; 190:398–408. [PubMed: 21689730]
13. Gabel LA, Marin I, Loturco JJ, Che A, Murphy C, Manglani M, Kass S. Mutation of the dyslexia-associated gene Dcdc2 impairs LTM and visuo-spatial performance in mice. Genes, Brain and Behavior. 2011; 10:868–875.
14. Centanni TM, Booker AB, Sloan AM, Chen F, Maher BJ, Carraway RS, et al. Knockdown of the Dyslexia-Associated Gene Kiaa0319 Impairs Temporal Responses to Speech Stimuli in Rat Primary Auditory Cortex. Cerebral Cortex. 2013 Advanced access.
15. Mainen ZF, Sejnowski TJ. Reliability of Spike Timing in Neocortical Neurons. Science. 1995; 268:1503–1506. [PubMed: 7770778]
16. Bean BP. The action potential in mammalian central neurons. Nat Rev Neurosci. 2007; 8:451–465. [PubMed: 17514198]
17. Clements J. Detection of spontaneous synaptic events with an optimally scaled template. Biophysical Journal. 1997; 73:220–229. [PubMed: 9199786]
18. Kayser C, Logothetis NK, Panzeri S. Millisecond encoding precision of auditory cortex neurons. Proc Natl Acad Sci USA. 2010; 107:16976–16981. [PubMed: 20837521]
19. Tiesinga P, Fellous JM, Sejnowski TJ. Regulation of spike timing in visual cortical circuits. Nat Rev Neurosci. 2008; 9:97–107. [PubMed: 18200026]
20. Panzeri S, Petersen RS, Schultz SR, Lebedev M, Diamond ME. The role of spike timing in the coding of stimulus location in rat somatosensory cortex. Neuron. 2001; 29:769–777. [PubMed: 11301035]
21. Butts DA, Weng C, Jin J, Yeh CI, Lesica NA, Alonso JM. Temporal precision in the neural code and the timescales of natural vision. Nature. 2007; 449:92–95. [PubMed: 17805296]
22. Harsch A, Robinson HPC. Postsynaptic variability of firing in rat cortical neurons: the roles of input synchronization and synaptic NMDA receptor conductance. J Neurosci. 2000; 57:1583–1589.

23. Sah P, Hestrin S, Nicoll RA. Tonic Activation of NMDA Receptors by Ambient Glutamate Enhances Excitability of Neurons. Science. 1989; 246:815–818. [PubMed: 2573153]
24. LoTurco JJ, Mody I, Kriegstein A. Differential activation of glutamate receptors by spontaneously released transmitter in slices of neocortex. Neuroscience letters. 1990; 114:265–271. [PubMed: 2169598]
25. Cecchi GA, Sigman M, Alonso J-M, Martinez L, Chialvo DR, Magnasco MO. Noise in Neurons Is Message Dependent. Proc Natl Acad Sci USA. 2000; 97:5557–5561. [PubMed: 10792057]
26. Cudmore RH, Fronzaroli-Molinieres L, Giraud P, Debanne D. Spike-Time Precision and Network Synchrony Are Controlled by the Homeostatic Regulation of the D-Type Potassium Current. Journal of Neuroscience. 2010; 30:12885–12895. [PubMed: 20861392]
27. Schoppa NE, Westbrook GL. Regulation of synaptic timing in the olfactory bulb by an A-type potassium current. Nat Neurosci. 1999; 2:1106–1113. [PubMed: 10570488]
28. Azouz R, Gray CM. Dynamic spike threshold reveals a mechanism for synaptic coincidence detection in cortical neurons in vivo. Proc Natl Acad Sci USA. 2000; 97:8110–8115. [PubMed: 10859358]
29. Tiesinga PHE, Sejnowski TJ. Rapid temporal modulation of synchrony by competition in cortical interneuron networks. Neural Comput. 2004; 16:251–275. [PubMed: 15006096]
30. Chance FS, Abbott LF, Reyes AD. Gain modulation from background synaptic input. Neuron. 2002; 35:773–782. [PubMed: 12194875]
31. Ermentrout GB, Galán RF, Urban NN. Reliability, synchrony and noise. Trends in Neurosciences. 2008; 31:428–434. [PubMed: 18603311]
32. Fellous JM, Rudolph M, Destexhe A, Sejnowski TJ. Synaptic background noise controls the input/output characteristics of single cells in an in vitro model of in vivo activity. Neuroscience. 2003; 122:811–829. [PubMed: 14622924]
33. Zsiros V, Hestrin S. Background Synaptic Conductance and Precision of EPSP-Spike Coupling at Pyramidal Cells. Journal of Neurophysiology. 2005; 93:3248–3256. [PubMed: 15716369]
34. Grosshans DR, Clayton DA, Coultrap SJ, Browning MD. LTP leads to rapid surface expression of NMDA but not AMPA receptors in adult rat CA1. Nat Neurosci. 2001; 5:27–33. [PubMed: 11740502]
35. Ngo-Anh TJ, Bloodgood BL, Lin M, Sabatini BL, Maylie J, Adelman JP. SK channels and NMDA receptors form a Ca^{2+}-mediated feedback loop in dendritic spines. Nat Neurosci. 2005; 8:642–649. [PubMed: 15852011]
36. Yuen EY, Jiang Q, Chen P, Gu Z, Feng J, Yan Z. Serotonin 5-HT_{1A} Receptors Regulate NMDA Receptor Channels through a Microtubule-Dependent Mechanism. Journal of Neuroscience. 2005; 25:5488–5501. [PubMed: 15944377]
37. Lipton SA, Rosenberg PA. Excitatory amino acids as a final common pathway for neurologic disorders. New England Journal of Medicine. 1994; 330:613–622. [PubMed: 7905600]
38. Lau CG, Zukin RS. NMDA receptor trafficking in synaptic plasticity and neuropsychiatric disorders. Nat Rev Neurosci. 2007; 8:413–426. [PubMed: 17514195]
39. Mozzachiodi R, Byrne JH. More than synaptic plasticity: role of nonsynaptic plasticity in learning and memory. Trends in Neurosciences. 2010; 33:17–26. [PubMed: 19889466]
40. O'Donnell P. Increased cortical excitability as a critical element in schizophrenia pathophysiology. Cortical Deficits In Schizophrenia. 2008:219–236.
41. Badawy RAB, Freestone DR, Lai A, Cook MJ. Epilepsy: Ever-changing states of cortical excitability. Neuroscience. 2012; 222:89–99. [PubMed: 22813999]
42. Lehongre K, Ramus F, Villiermet N, Schwartz D, Giraud A-L. Altered low-3 sampling in auditory cortex accounts for the three main facets of dyslexia. Neuron. 2011; 72:1080–1090. [PubMed: 22196341]
43. Ramus F. Developmental dyslexia: specific phonological deficit or general sensorimotor dysfunction? Current Opinion in Neurobiology. 2003; 13:212–218. [PubMed: 12744976]
44. McAnally KI, Stein JF. Auditory temporal coding in dyslexia. Proc Biol Sci. 1996; 263:961–965. [PubMed: 8805833]

45. Czamara D, Bruder J, Becker J, Bartling J, Hoffmann P, Ludwig KU, et al. Association of a Rare Variant with Mismatch Negativity in a Region Between KIAA0319 and DCDC2 in Dyslexia. Behav Genet. 2010; 41:110–119. [PubMed: 21104116]
46. Gaab N, Gabrieli JDE, Deutsch GK, Tallal P, Temple E. Neural correlates of rapid auditory processing are disrupted in children with developmental dyslexia and ameliorated with training: an fMRI study. Restor Neurol Neurosci. 2007; 25:295–310. [PubMed: 17943007]
47. Goswami U. A temporal sampling framework for developmental dyslexia. Trends in Cognitive Sciences. 2011; 15:3–10. [PubMed: 21093350]
48. Vandermosten M, Boets B, Luts H, Poelmans H, Golestani N, Wouters J, Ghesquière P. Adults with dyslexia are impaired in categorizing speech and nonspeech sounds on the basis of temporal cues. Proc Natl Acad Sci USA. 2010; 107:10389–10394. [PubMed: 20498069]
49. Ahissar M, Protopapas A, Reid M, Merzenich MM. Auditory processing parallels reading abilities in adults. Proc Natl Acad Sci USA. 2000; 97:6832–6837. [PubMed: 10841578]
50. Engineer CT, Perez CA, Chen YH, Carraway RS, Reed AC, Shetake JA, et al. Cortical activity patterns predict speech discrimination ability. Nat Neurosci. 2008; 11:603–608. [PubMed: 18425123]
51. Tchumatchenko T, Malyshev A, Wolf F, Volgushev M. Ultrafast Population Encoding by Cortical Neurons. Journal of Neuroscience. 2011; 31:12171–12179. [PubMed: 21865460]
52. Tiesinga PHE, Toups JV. The possible role of spike patterns in cortical information processing. J Comput Neurosci. 2005; 18:275–286. [PubMed: 15830164]
53. Taylor KR, Holzer AK, Bazan JF, Walsh CA, Gleeson JG. Patient mutations in doublecortin define a repeated tubulin-binding domain. J Biol Chem. 2000; 275:34442–34450. [PubMed: 10946000]
54. Coquelle FM, Levy T, Bergmann S, Wolf SG. The DCX Superfamily 1: Common and Divergent Roles for Members of the Mouse DCX Superfamily. Cell. 2006
55. Dijkmans TF, van Hooijdonk A, Wilhelmina L, Fitzsimons CP, Vreugdenhil E. The doublecortin gene family and disorders of neuronal structure. Central Nervous System Agents in Medicinal Chemistry. 2010; 10:32–46. [PubMed: 20236041]
56. Corlew R, Wang Y, Ghermazien H, Erisir A, Philpot BD. Developmental Switch in the Contribution of Presynaptic and Postsynaptic NMDA Receptors to Long-Term Depression. Journal of Neuroscience. 2007; 27:9835–9845. [PubMed: 17855598]
57. Brasier D, Feldman DE. Synapse-Specific Expression of Functional Presynaptic NMDA Receptors in Rat Somatosensory Cortex. J Neurosci. 2008
58. Kunz PA, Roberts AC, Philpot BD. Presynaptic NMDA Receptor Mechanisms for Enhancing Spontaneous Neurotransmitter Release. Journal of Neuroscience. 2013; 33:7762–7769. [PubMed: 23637168]
59. Ludwig KU, Roeske D, Herms S, Schumacher J, Warnke A, Plume E, et al. Variation in GRIN2Bcontributes to weak performance in verbal short-term memory in children with dyslexia. Am J Med Genet. 2009; 153B:503–511. [PubMed: 19591125]

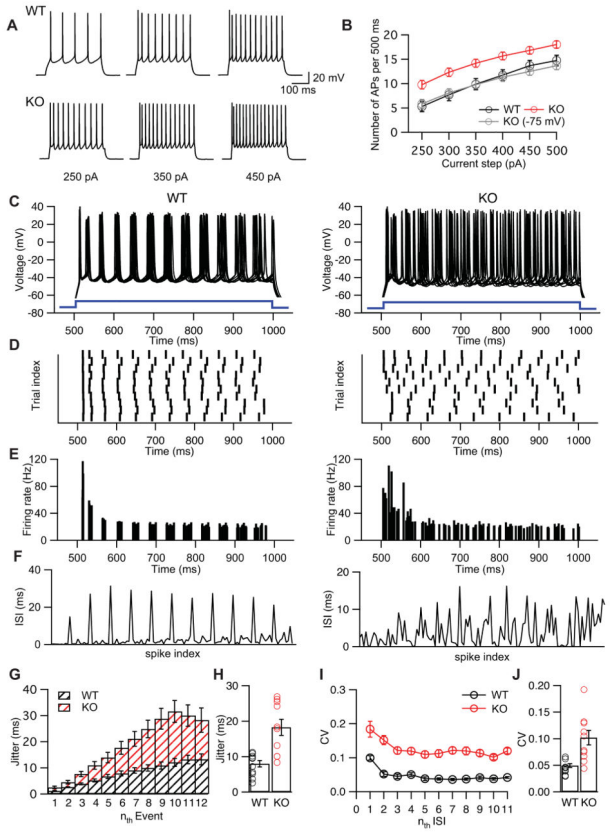

Figure 1. Dcdc2 KO neurons have increased spike rates and spike-time variability

(A) Action potential trains elicited by 250 (left), 350 (middle), and 450 pA (right) current steps in a WT (top) and a KO neuron (bottom). **(B)** Average number of APs generated by 500 ms current steps from 250 pA to 500 pA at 50 pA increments in WT (black), KO (red), and KO neurons with RMP adjusted to −75 mV with holding current (gray). Repeated measures ANOVA, between variables: condition (WT, KO, and KO at −75 mV), within variables: current step (250, 300, 350, 400, 450, 500 pA); main effect of condition: $F(2,49) = 6.30$, $P < 0.005$; followed by Dunnett's test, difference significant between WT and KO for all 6 current steps, no significance between WT and KO (−75 mV) for all 6 current steps. WT: n = 16, KO: n = 22, KO (−75 mV): n = 14. **(C)** Spike trains were evoked by 500 ms dc current injection and voltage traces from ten trials were overlaid for a WT (left) and a KO (right) neuron. Stimulus waveforms are indicated in blue. RMPs for recorded neurons were adjusted to −75 mV by constant current injection, and 12-spike AP trains for both conditions was achieved by adjusting the amplitude of current step. Correspondent **(D)** rastergrams and **(E)** histograms of instantaneous firing rate for a representative WT (left) and KO (right) neuron. Spikes from all ten trials were ordered according to their peak times, and histograms of ISIs between subsequent peaks were shown in **(F). (G)** Temporal jitter (the standard deviation of spike times for each event) for KO (red) and WT (black) neurons. Repeated measures ANOVA, between variables: genotype (WT and KO); within variables: event (1 to 12^{th} event); genotype x event interaction: $F(11, 198) = 8.38$, $p < 0.0001$. **(H)** the average jitter, or the main effect of genotype on jitter: $F(1,18) = 12.14$, $P < 0.005$. The significant interaction between genotype and event is likely due to the accumulation of increased jitter

towards later spikes. Holm-Sidak's test, no significance between WT and KO jitter: 1st to 6th event; significant different: 7th to 12th event. **(I)** The coefficient of variance (CV) of inter-spike intervals (ISIs) for each event in WT and KO neurons. Repeated measures ANOVA, between variables: genotype (WT and KO); within variables: event (1st to 11th ISI), followed by Holm-Sidak's test, difference significant between genotypes for all 11 ISIs. **(J)** the average jitter, or the main effect of genotype: $F(1,18) = 22.76$, $P < 0.0005$. Circles in **(H)** and **(J)** indicate collapsed averages from individual neurons. Error bars indicate SEM. WT: n = 10, KO: n = 10.

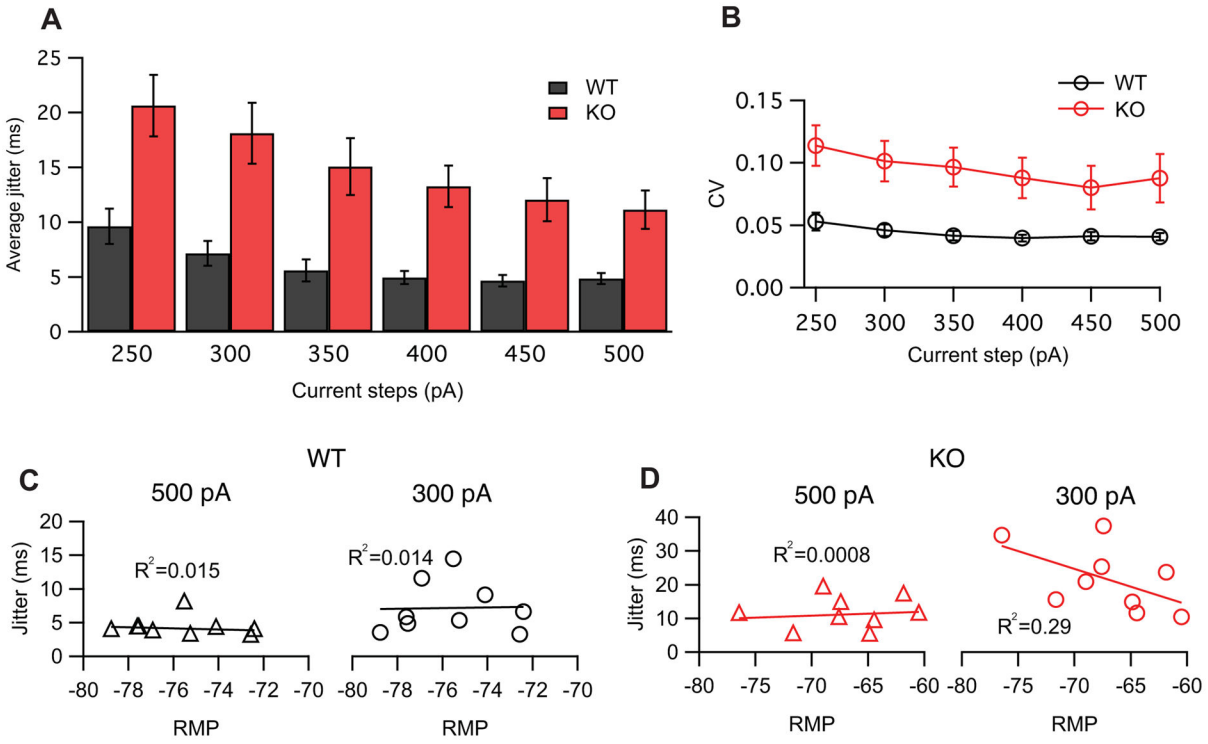

Figure 2. Decreased spike-time precision in Dcdc2 KO neurons is not a result of altered excitability and RMP

(A) Average jitter for WT (dark grey bars) and KO (red bars) neurons at 250, 300, 350, 400, 450, and 500 pA current injection. Repeated measures ANOVA (between variables: genotype; within variables: current step), main effects of genotype: $F(1,16) = 16.14$, $P < 0.001$; followed by Holm-Sidak's test, difference significant between genotypes for all 6 current steps. **(B)** Average CV for WT (black) and KO (red) neurons. Repeated measures ANOVA (between variables: genotype; within variables: current step), main effects of genotype: $F(1,16) = 9.62$, $P < 0.01$; followed by Holm-Sidak's test, difference significant between genotypes for all 6 current steps. Average jitter was not correlated with RMP in **(C)** WT or **(D)** KO neurons at 300 pA and 500 pA current step (linear regression, R^2 values of best fitted lines indicated on graphs). Error bars indicate SEM. WT, n = 9; KO, n = 9.

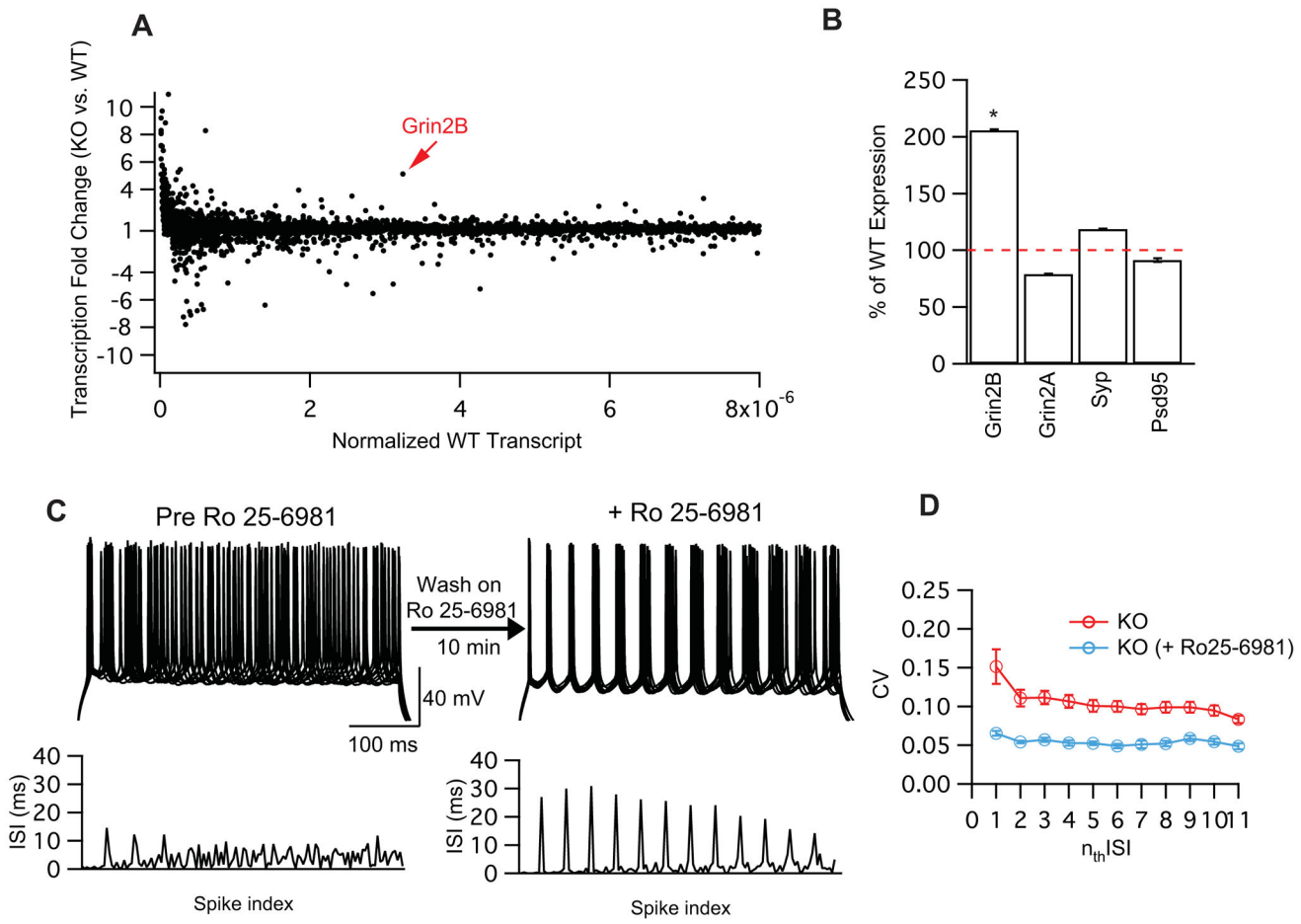

Figure 3. Dcdc2 KOs show elevated Grin2B expression and improved spike-time precision by NMDAR2B-specific antagonist Ro 25-6981

(A) RNA-seq profile of transcribed genes in P22 mouse forebrain. Transcription fold change (number of normalized reads in KO relative to reads in WT for each gene) was plotted against normalized WT transcript reads. Grin2B is indicated by red arrow. **(B)** Expression levels of Grin2B, Grin2A, Synaptophysin (Syp) and Psd95 determined by qRT-PCR. Grin2B WT vs. KO: Student's t-test, $P < 0.0005$. WT and KO: n = 6. Grin2A, Syp and Psd95 were not differentially regulated in RNA-seq, and also not significantly different from WT expression levels by qRT-PCR. **(C)** Representative spike trains and ISI histograms of a Dcdc2 KO neuron pre (left) and post (right) washing on Ro 25-6981 (0.5 μM). Spike trains were evoked by 500 ms dc current input and voltage traces from 15 trials were overlaid. Twelve-spike AP trains for both conditions was achieved by adjusting the amplitude of current step. **(D)** Mean effect of Ro 25-6981 on CV of ISIs of 12-spike trains in KO neurons. Repeated measures ANOVA, matching: event (1^{st} to 11^{th} ISI) and treatment (pre Ro 25-6981 and in Ro 25-6981), main effect of treatment: $F(1,6) = 9.40$, $P < 0.005$. Error bars indicate SEM. KO, n = 7.

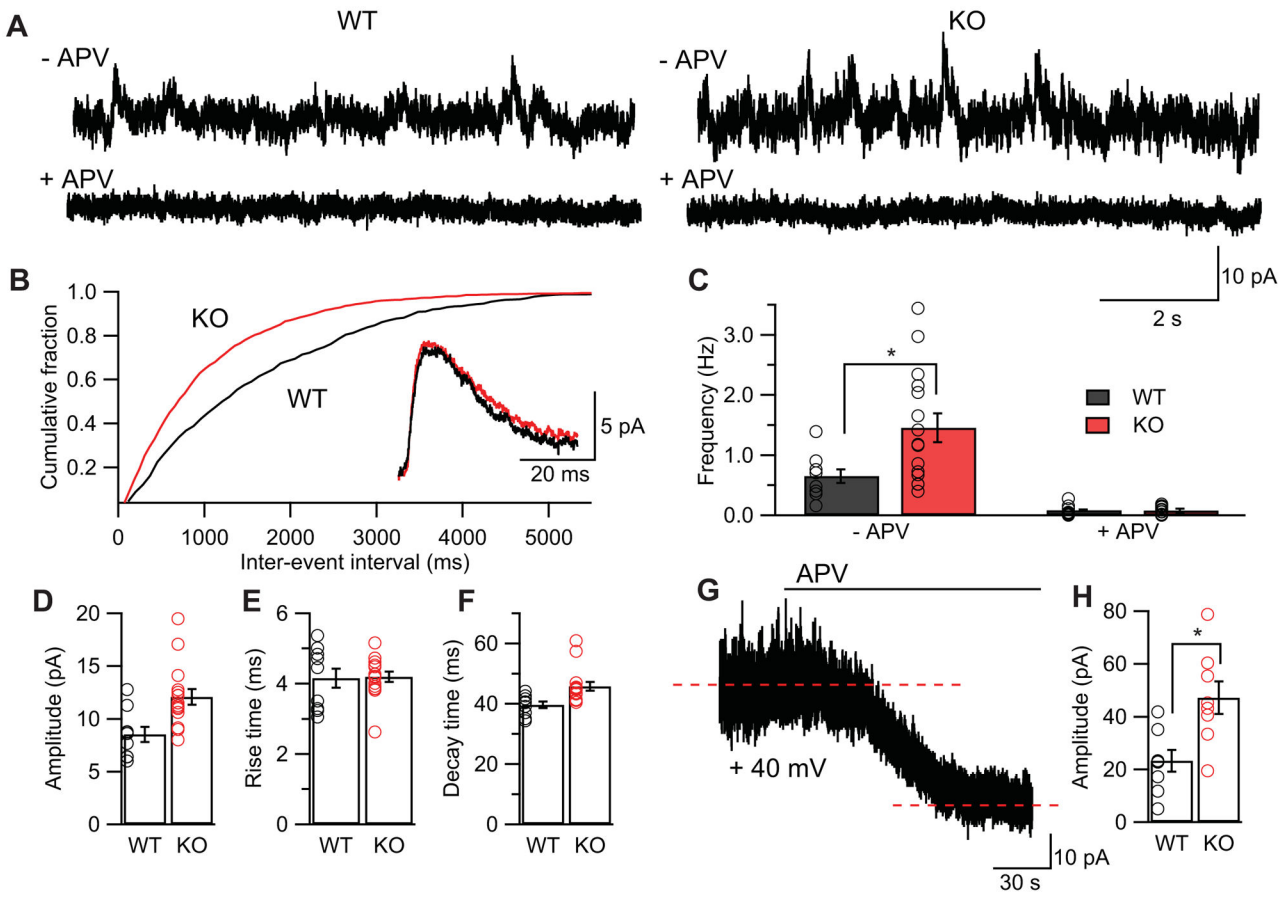

Figure 4. Dcdc2 KO neurons show more spontaneous NMDAR activity compared to WT neurons

(A) Representative traces illustrate spontaneous NMDAR-mediated currents recorded at +40 mV in normal recording solution (top) and after washing on DL-APV (100 μM, bottom) for WT (left) and Dcdc2 KO (right) neurons. **(B)** Cumulative probability histogram for inter-event interval of NMDAR-mediated events in normal recording solution for WT and KO neurons. The histogram is a mean of individual histograms from all cells recorded in both conditions. Inset, average waveform across the population (WT: black, KO: red) **(C)** Comparison of phasic NMDAR-mediated event frequencies in WT versus KO neurons. Student's t-Test, t (22) = 2.46, $P < 0.05$; WT, n = 9; KO, n =15. Bath application of APV abolished NMDAR-mediated spontaneous events in the same WT or KO neurons. **(D)** Mean amplitude [t (22) = 1.54, NS], **(E)** rise time [t (22) = 0.13, NS], and **(F)** decay time [t (22) = 0.38, NS] of WT and KO neurons were not significantly different. **(G)** Representative trace of the change in NMDAR-mediated tonic current and current variance during the application of APV at holding potential of +40 mV in a KO neuron. Dotted lines indicate baseline averages. **(H)** Comparison of the change in mean tonic current pre and post APV in WT and KO neurons. Student's t-test, t (14) #x0003D; 3.23, $P < 0.01$. WT: n=8, KO: n=8. Circles indicate measurements from individual neurons. Error bars indicate SEM.

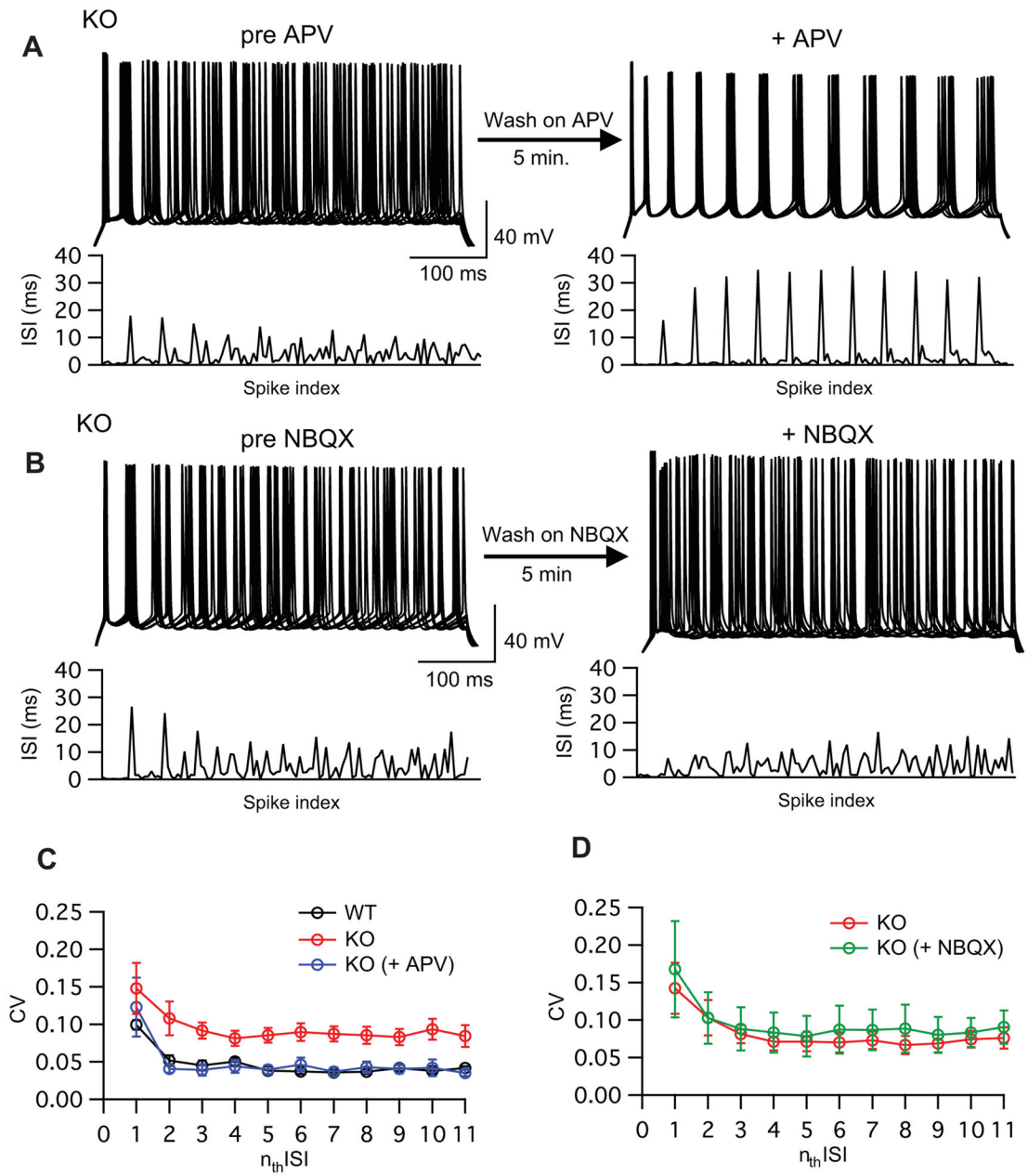

Figure 5. Blockade of NMDAR but not AMPAR restores spike timing variability in KO neurons

Representative spike trains and ISI histograms of a Dcdc2 KO neuron pre (left) and after (right) washing on **(A)** DL-APV (100 μM) and **(B)** NBQX (1 μM). Spike trains were evoked by 500 ms dc current input and voltage traces from 15 trials were overlaid. Twelve-spike AP trains for both conditions was achieved by adjusting the amplitude of current step. **(C)** Mean effect of APV on CV of ISIs of 12-spike trains in KO neurons. KO pre vs. in APV: repeated measures ANOVA, matching: event (1^{st} to 11^{th} ISI) and treatment (pre APV and in APV); main effect of treatment: F (1,9) = 40.26, $P < 0.005$. KO in APV vs. WT: repeated measures ANOVA, between variables: genotype (WT and KO); within variables: event (1^{st} to 11^{th} ISI); main effects of genotype: F (1,18) = 0.67, NS. WT, n = 10; KO, n = 10. **(D)** Mean

effect of NBQX on CV of ISIs a 12-spike train in KO neurons. Repeated measures ANOVA, matching: event (1^{st} to 11^{th} ISI) and treatment (pre NBQX and in NBQX); main effect of treatment: $F(1,9) = 0.16$, NS. WT: n=10, KO: n=10. Error bars indicate SEM.

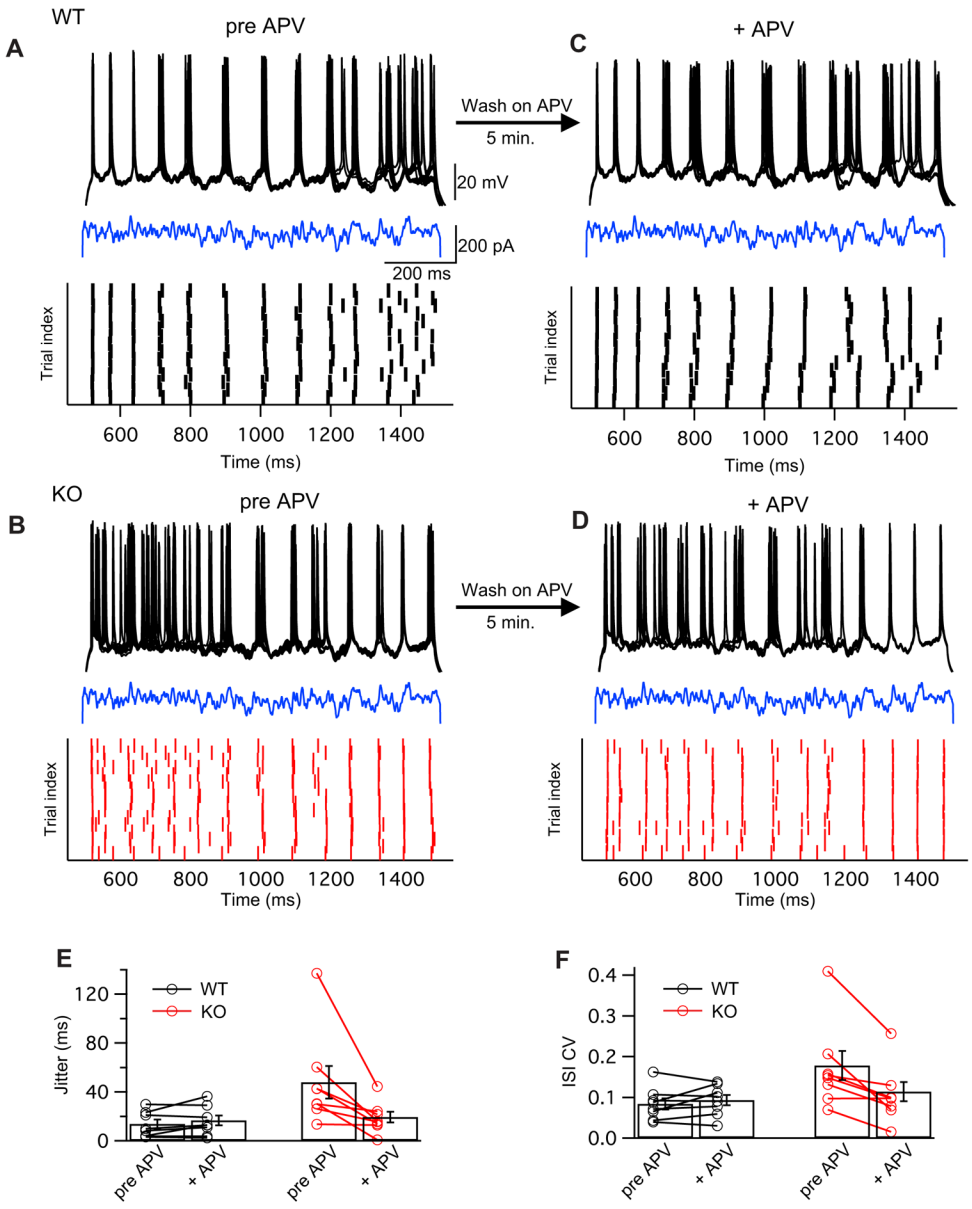

Figure 6. Blockade of NMDAR restores spike-time precision of KO spike trains elicited by fluctuating current

A frozen noise stimulus (shown in blue; Gaussian white noise, μ_s = 200 pA, σ_s = 100 pA, and τ_s = 3 ms) was applied repeatedly to evoke action potential trains. Overlaid voltage traces and rastergrams in a representative **(A)** WT and a **(B)** KO neuron. Spike trains and rastergrams of the same **(C)** WT and **(D)** KO neurons after washing on DL-APV (100 μM). **(E)** Effect of washing on APV on average WT jitter (black) versus KO jitter (red). Circles connected with lines indicate jitter measurement of the same cell before and after APV. Repeated measures ANOVA, between variables: genotype (WT and KO), within variables: treatment (pre APV and in APV); genotype x treatment interaction: $F(1,14) = 9.40$, $P < 0.01$; followed by Sidak's test, difference significant between genotypes pre APV, no significance in APV **(F)** Effect of washing on APV on average ISI CV in WT (black) versus

ISI CV in KO (red). Circles connected with lines indicate CV calculated for the same cell before and after APV. Repeated measures ANOVA, between variables: genotype, within variables: treatment, genotype x treatment interaction: $F(1,14) = 13.34$, $P < 0.005$; followed by Sidak's test, difference significant between genotypes pre APV, no significance in APV. Bars indicate averages and error bars indicate SEM. WT, n = 8; KO, n = 8.

Table 1

Electrophysiological properties of WT and Dcdc2 RS neurons

Membrane properties	**WT cells (n = 21)**	**Dcdc2 KO cells (n = 25)**
V_{rmp}* (mV)	−74.50 ± 0.88	−68.94 ± 1.19
R_{input}* (MΩ)	91.72 ± 7.74	125.20 ± 11.35
G_{slope}* (nS)	17.38 ± 0.08	11.13 ± 0.11
Action potential properties	WT cells (n = 11)	Dcdc2 KO cells (n = 11)
Rise time (ms)	0.23 ± 0.01	0.21 ± 0.01
Width (ms)	0.93 ± 0.06	0.84 ± 0.05
Threshold (mV)	−37.65 ± 1.02	−38.69 ± 0.63
Peak (mV)	42.17 ± 2.00	42.61 ± 1.84
Max. rate of rise (mV/ms)	218.00 ± 11.63	228.20 ± 7.63

Data are means ± standard error.

Asterisks indicate properties that are significantly different between WT and KO neurons.